Письма в ЭЧАЯ. 2008. Т. 5, № 1(143). С. 28–39

JET ENERGY MEASUREMENTS IN CMS

O. L. Kodolova

Skobeltsyn Institute of Nuclear Physics of the Moscow State University, Moscow

The expected performance of CMS for jet energy measurements is discussed. The use of the different calibration methods allows one to restore the linearity of the CMS calorimeter relative to jets and to improve the jet energy resolution.

Рассматривается возможность восстановления энергии жестких струй на установке CMS с использованием как калориметрической системы, так и других детекторных систем, входящих в состав установки. Описаны методы коррекции энергии струй, собранной в калориметре, позволяющие улучшить линейность отклика и энергетическое разрешение.

PACS: 06.90.+v

INTRODUCTION

Event signatures for SUSY, Higgs boson production, and other new physics processes require the reconstruction and measurement of jets coming from high-momentum quarks and gluons. The jet energy resolution and linearity are key factors in separating signal events from background and in measuring the properties of the signal.

An example of jet reconstruction in a hard interaction forming QCD dijets, with its characteristic features, is shown in Fig. 1. The parameters of the initial parton corresponding

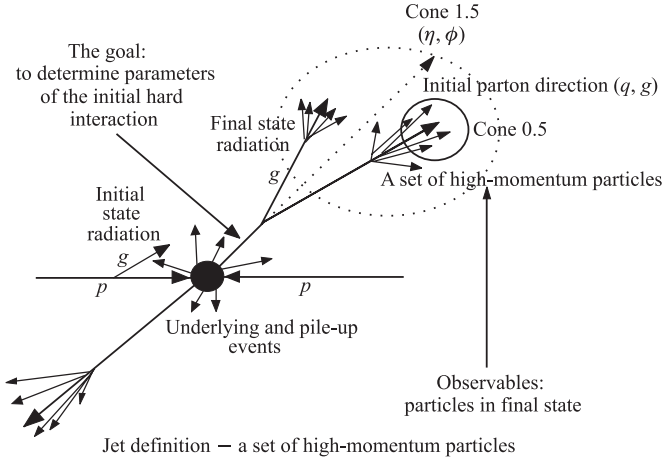

Fig. 1. Complexities in the jet definition arise from several processes including final state radiation, underlying event fragments and the detector-level collection of particle energies

to the particle jet depend on a number of factors including final state radiation, which can lead to the splitting of the jet in the detector. Taking a large cone of $R = 1.5$ in η, ϕ, the jet reconstruction collects a large fraction of the energy of the initial parton. Such a cone is also susceptible to collecting the energy of non-isolated additional partons in the hard interaction in addition to energy from the underlying event, pile-up interactions and electronic noise.

1. CMS DETECTOR

A characteristic feature of the CMS detector is its large superconducting solenoid delivering an axial magnetic field of 4 T [1].

Detector has tracker, electromagnetic (ECAL) and hadronic (HCAL) calorimeters and muon chambers. The hadron and electromagnetic calorimeters are located inside the coil (except the forward calorimeter) and cover the pseudorapidity range $|\eta| < 5$ [1]. Electromagnetic calorimeter consists of 76000 crystals of $PbWO_4$ and covers the range $|\eta| < 3$. The granularity of the crystals in the ECAL barrel is $\Delta\eta \times \Delta\phi = 0.0175 \times 0.0175$ rad, which corresponds to a crystal front face of about 20×20 mm. In the ECAL endcap ($1.48 < |\eta| < 3.0$), the (η, ϕ) granularity increases progressively to a maximum value of $\Delta\eta \times \Delta\phi = 0.05 \times 0.05$ rad, while the crystal size of 28×28 mm remains the same. Crystals have length 230 mm (25.8 radiation length) in barrel ($|\eta| < 1.48$) and 220 mm (24.7 radiation length) in endcap ($|\eta| > 1.48$). In endcap, the preshower is located in front of the ECAL.

The HCAL barrel is composed of flat brass alloy absorber plates parallel to the beam line. Innermost and outermost plates are made of stainless steel for structural strength. There are 17 active plastic scintillator tiles interspersed between the stainless steel and brass absorber plates. The first and the last scintillator tiles are 9 mm, the other tiles are of 3.7 mm. The thickness of absorber plates differs from 50.5 to 75 mm.

The HCAL endcap calorimeter ($1.305 < |\eta| < 3.0$) is composed entirely of brass absorber plates. The thickness of plates is 78 mm, while the scintillator thickness is 3.7 mm, hence reducing the sampling fraction. There are 19 active scintillator layers. The overlapping region of the HCAL barrel and endcap is $1.305 < |\eta| < 1.74$. There is no longitudinal segmentation in the ECAL and in the barrel part of the HCAL, except in the barrel–endcap transition region.

The full number of nuclear interaction length in the range $|\eta| < 3$ is varying from 11 to 16. The ratio e/h measured at test-beams is in the range 1.3–1.4 [2, 3].

The forward calorimeters (HF) are located 11.2 m from interaction point. They are made of steel absorber and embedded radiation hard quartz fibers, which provide the fast collection of Cherenkov light. The quartz fibers have width of 1 mm and are located at a distance of 5 mm from each other. To separate hadronic and electromagnetic showers, short (143 cm) and long (165 cm) quartz fibers are used. The e/h ratio is 5 for HF [4]. The full number of radiation length of HF is 25.

The calorimeters are designed to allow jet reconstruction in the full pseudorapidity region. The calorimeter extends to $\eta = 5$, but jets can be measured if their axes lie in the range $|\eta| < 4.5$. At $\eta = 5$, half the jet will be lost.

In the barrel and most of the endcap part of HCAL, the size of the towers is $\Delta\eta = 0.0870$ by $\Delta\phi = 2\pi/72 \approx 0.0873$ rad. At high η in the HCAL endcap ($|\eta| > 1.74$), the towers become larger in η (from 0.087 to 0.175) and double the size in ϕ.

Since the ECAL granularity is much finer than HCAL, calorimeter tower (ECAL plus HCAL) is formed by addition of signals in η, ϕ bins corresponding to individual HCAL cells.

The size of calorimeter tower of forward calorimeters ($3.0 < |\eta| < 5.0$) is 0.175×0.175 except the first tower (0.111) and the last one (0.3).

During the data acquisition the cut on energy is applied to HCAL towers to keep the occupancy on the level of 15%. Only HCAL towers with energy more than 0.5 GeV after the baseline subtraction (1.2 GeV) are kept for the further processing. The read-out of the ECAL cells is more complicated and is described in detail in [6].

The tracker is covered in the range $|\eta| < 2.4$ and is composed of two different types of detectors, pixels and silicon strips. The tracker system allows one to measure p_T of charged particles with accuracy better than 2% in the momentum range from 0.5 GeV to a few tens GeV in the range $|\eta| < 1$.

2. JET RECONSTRUCTION

The first step in the reconstruction, before invoking the jet algorithm, is to apply noise and pile-up suppression.

The second step is to apply one of the jet finding algorithms (iterative cone algorithm, middle point algorithm or K_T algorithm [5–8]) and to get the jet energy and position.

The factors influencing the reconstructed jet energy can be divided into two groups. In addition to the factors shown in Fig. 1 and connected with the jet as a physical object jets are affected by the detector performance, e.g., electronic noise, magnetic field which deflects low-energy charged particles out of the jet reconstruction cone, the responses of the calorimeters to electromagnetic and hadronic showers (e/h ratio), and some other sources of the energy loss. While many of the corrections for effects in the first group are channel-dependent, the bulk of the detector effects is more channel-independent and common correction coefficients can be provided.

At the third step the calibration methods are applied to restore a correspondence in the measured jet properties between matched reconstructed and particle-level jets.

3. JET CALIBRATION

Algorithms for jet energy corrections may be classified according to the different objects that are used for the corrections.

Jet-based corrections are implemented by weighting the energies from the longitudinal calorimeter compartments.

Cluster-based coefficients are applied separately to electromagnetic and hadronic clusters, separated according to the cluster origin (electron, γ, hadron).

As for track-based corrections, the tracks that are deflected from the jet region due to magnetic field can be added to the jet energy reconstructed in calorimeter. The response of charged particles within the jet area can be changed to the momentum (energy) of the tracks giving impact on the ECAL surface inside the jet region.

3.1. Monte-Carlo Calibration of Jet Response (Jet Based) [12]. The events are simulated with one of the Monte-Carlo programs tunned for the dedicated energy and are passed through the detailed model of detector [12]. The jets are reconstructed with one of the jet finding algorithms. Particle-level jets are found by applying the same jet algorithm to stable particles (excluding neutrinos and muons). A matching criterion, based on the distance $\Delta R = \sqrt{d\eta^2 + d\varphi^2} < 0.2$, is used to associate particle-level and reconstructed jets [12]. The ratio of reconstructed jet transverse energy to the particle-level jet transverse energy as a function of the particle-level jet transverse energy is approximated by the set of functions for the different η regions. Further, these curves are used as weights to the reconstructed jet energy to provide the corrected jet energy.

A sample of PYTHIA [11] events was simulated in the narrow $\hat{p}_T$ in the energy range from 0 to 3500 GeV. The response of the detector was obtained with the detailed model of the detector in the low-luminosity conditions ($\mathcal{L} = 2 \cdot 10^{33}$ cm$^{-2} \cdot$ s^{-1}) using the CMS simulation program based on GEANT4 [10].

Jets were reconstructed with the additional threshold on the calorimeter tower $E_T > 0.5$ GeV, $E > 0.8$ GeV, i.e., only calorimeter towers above threshold contribute to the jet energy. The dependence of the transverse momentum of jet on the additional threshold applied to the calorimeter towers was studied [12]. The response of the jet with generated transverse energy of 20 GeV is 15 GeV if no additional threshold is applied. After applying the threshold $E_T > 0.5$ GeV the response to the 20 GeV jet falls down to 10 GeV. The further increasing threshold ($E_T > 0.5$ GeV, $E > 0.8$ GeV) leads to the response of 8.5 GeV. This dependence is the consequence of the nonuniform distribution of the jet in the cone (radius 0.5 corresponds to 120 calorimeter towers) and the signal in the towers is compared with electronic noise. One has to mention that thresholds introduce the additional nonlinearity in the calorimeter response to jets, since whether the tower contributes into jet energy depends on the sum of the signal energy and noise in this tower (1):

$$\langle E_{\text{jet}} \rangle = \frac{1}{N_{\text{events}}} \sum_{N_{\text{events}}} \sum_{(E_{\text{tower}} + E_{\text{noise}} - \langle E_{\text{noise}} \rangle) > E_{\text{cut}}} (E_{\text{tower}} + E_{\text{noise}} - \langle E_{\text{noise}} \rangle). \quad (1)$$

The reconstructed energy starts to depend on the jet shape, the jet content and the jet energy.

The jet energy linearity before and after applying Monte-Carlo corrections and resolution after applying Monte-Carlo corrections are shown in Figs. 2, 3 for the iterative cone algorithm with $R = 0.5$ and the threshold applied to the calorimeter tower equal to $E_T > 0.5$ GeV, $E > 0.8$ GeV.

The jet energy resolution is presented for the three ranges $|\eta| < 1.4$, $1.4 < |\eta| < 3.0$, $3.0 < |\eta| < 5.0$. The mean values and dispersions are got by means of fit of the distributions $E_T^{\text{rec}}/E_T^{\text{MC}}$ with Gaussian. For the low-energy jets the distribution is not symmetric and the fit is done in the range of maximum ($\pm\sigma$).

The resolution is parametrized with the expression

$$\frac{\sigma(E_T^{\text{rec}}/E_T^{\text{MC}})}{\langle E_T^{\text{rec}}/E_T^{\text{MC}} \rangle} = \frac{a}{E_T^{\text{MC}}} \oplus \frac{b}{\sqrt{E_T^{\text{MC}}}} \oplus c, \quad (2)$$

where the first term is due to fixed energy fluctuations in the cone from electronic noise, pile-up and underlying event energy, the second term comes from the stochastic response

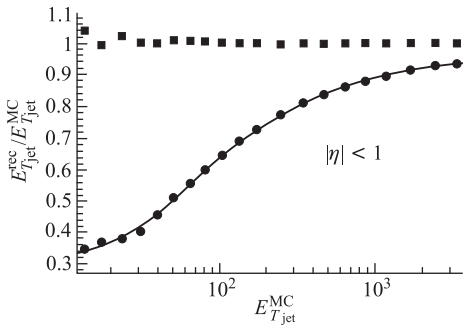

Fig. 2. The ratio of the reconstructed jet transverse energy $E_T^{\rm rec}$ to the generated transverse energy $E_T^{\rm MC}$ as a function of $E_T^{\rm MC}$ for jets with $|\eta_{\rm jet}| < 1$ reconstructed by the iterative cone $R = 0.5$ algorithm before (circles) and after (squares) MC jet calibration [12]

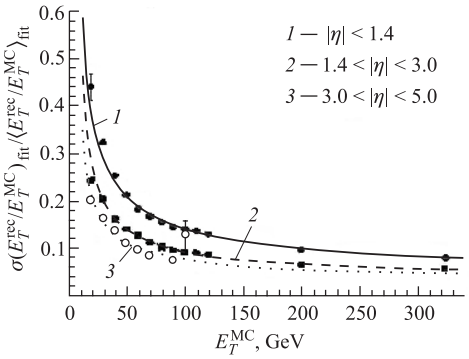

Fig. 3. The jet energy resolution as a function of generated jet energy for the different pseudorapidity intervals after applying corrections on the jet energy [12]

Jet energy resolution parameters in 3η regions of the calorimeters for the iterative cone $R = 0.5$

IC, $dR < 0.2$	$\lvert\eta\rvert < 1.4$ (EB + HB + HO)	$1.4 < \lvert\eta\rvert < 3.0$ (EE + HE)	$3.0 < \lvert\eta\rvert < 5.0$ (HF)
Before correction	$\frac{7.5}{E_T^{\rm MC}} \oplus \frac{1.44}{\sqrt{E_T^{\rm MC}}} \oplus 0.034$	$\frac{8.5}{E_T^{\rm MC}} \oplus \frac{0.67}{\sqrt{E_T^{\rm MC}}} \oplus 0.049$	$\frac{4.1}{E_T^{\rm MC}} \oplus \frac{0.2}{\sqrt{E_T^{\rm MC}}} \oplus 0.087$
After correction	$\frac{5.6}{E_T^{\rm MC}} \oplus \frac{1.25}{\sqrt{E_T^{\rm MC}}} \oplus 0.033$	$\frac{4.8}{E_T^{\rm MC}} \oplus \frac{0.89}{\sqrt{E_T^{\rm MC}}} \oplus 0.043$	$\frac{3.8}{E_T^{\rm MC}} \oplus 0.085$

of the calorimeter measurements, and the last term is the constant term from residual non-uniformities and nonlinearities in the detector response. The fit is done down to a transverse energy of 30 GeV in barrel and endcap and of 20 GeV in very forward region. The result of the fits are presented in the table. The MC jet calibration takes into account the geometry of detector and improves the resolution in barrel region. This type of corrections can be used for tuning the Monte-Carlo generators with data.

3.2. The Calibration of Jet Response with $\gamma+$ Jet Channel (Jet Based) [13]. The channels of $\gamma/Z+$ jet and $W \to jj$ (from $t\bar{t}$ production) will give the first estimation of the absolute energy scale [13]. The jet energy scale is set using the kinematics relationship of transverse momentum balancing between the direct photon and the jet. The measured observable $k_{\rm jet} \equiv P^{\rm jet}_{T\rm meas}/P^{\gamma}_{T}$ provides an approximate value for the true parton-level calibration of the jet given by $k^{\rm true}_{\rm jet} \equiv P^{\rm jet}_{T\rm meas}/P^{\rm parton}_{T}$. The systematic shifts introduced by the difference between gluon and quark jets are presented in Fig. 4.

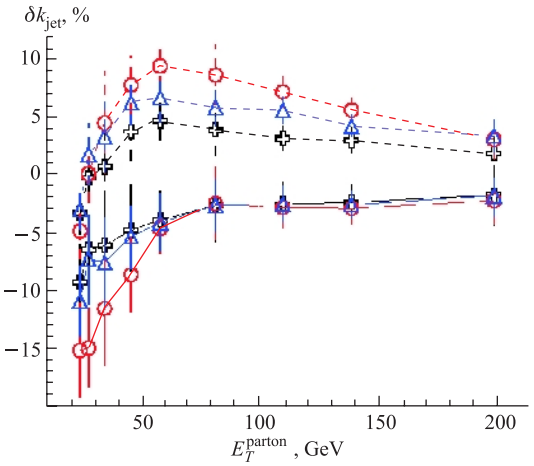

Fig. 4. Relative systematic errors $((k_{\text{jet}} - k_{\text{jet}}^{\text{true}})/k_{\text{jet}}^{\text{true}})$ on the calibration of the jets initiated by the light quarks (solid lines) and the jets from the QCD sample (including gluons) (dashed lines) for the iterative cone algorithm with cone radii of $R = 0.5$ (circles) and $R = 0.7$ (triangles) and for the K_T-cluster algorithm using the E_T-scheme (crosses) for the $E_T^{\text{tower}} > 0.5$ GeV [13]

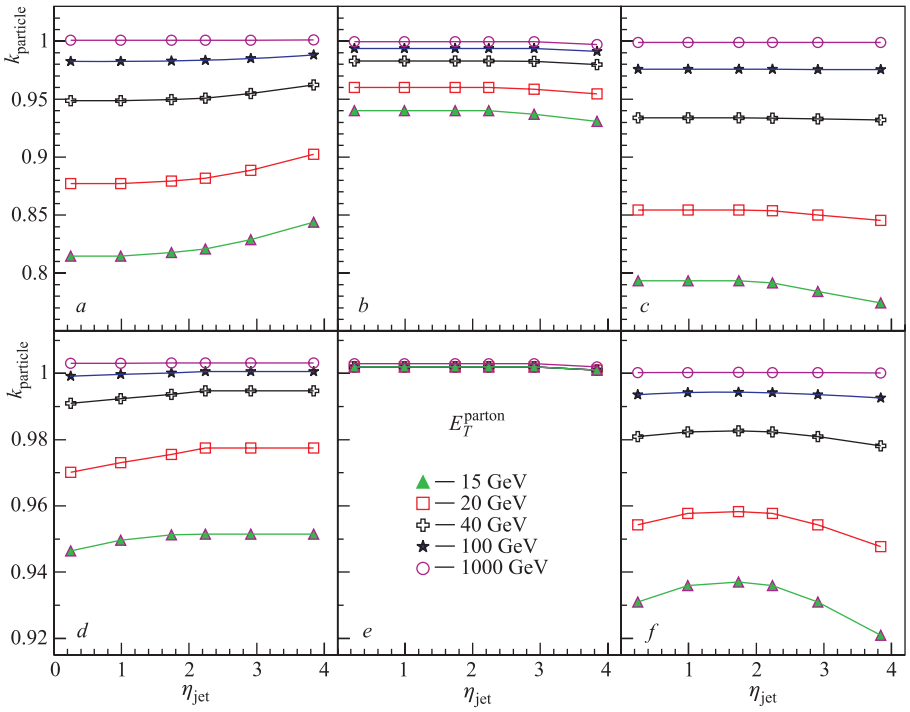

Fig. 5. Ratio of transverse momenta of particle jets to the transverse momenta of the initial partons for QCD (a, d), quark (b, e) and gluon (c, f) jets collected in cones of $R = 0.5$ (a, b, c) and $R = 0.7$ (d, e, f) [13]

The correction with $\gamma + \mathrm{jet}$ channel can be applied to particle jet with the additional MC correction taking into account the difference between parton and particle jet: $E^{\mathrm{jet}}_{T\mathrm{particle}} = E^{\mathrm{parton}}_{T\mathrm{jet}} \times k^{\mathrm{particle}}_{\mathrm{jet}}$. The difference between parton and jet on the particle level is presented in Fig. 5 for the different samples.

The jets initiated by quarks are more collimated than those initiated by gluons. All energy of parton at all energies can be collected in the cone with $R > 1$ for gluon jets and $R = 0.7$ for quark jets (Fig. 5).

3.3. The Calibration of Jet Response with the Use of Tracks [14]. A response subtraction procedure was proposed in Ref. [14]. For each track reaching the calorimeter surface within the reconstruction jet area the expected response is subtracted from the calorimeter jet energy and the track momentum is used instead. This subtraction procedure does not require cluster separation and therefore is well suited to the case of high occupancy or coarse granularity. The momenta of the tracks that reach the calorimeter surface out of the reconstruction cone are simply added to the calorimeter jet energy.

Before the subtraction, the reconstructed jet energy is

$$E^{\mathrm{rec}}_{\mathrm{jet}} = \mathrm{EC}_{e/\gamma} + (\mathrm{EC} + \mathrm{HC})_{\mathrm{neut.\ hadr.}} + (\mathrm{EC} + \mathrm{HC})_{\mathrm{charg.\ hadr.}}, \tag{3}$$

where $(\mathrm{EC} + \mathrm{HC})_{\mathrm{neutr.\ hadr.}}$ and $(\mathrm{EC} + \mathrm{HC})_{\mathrm{charg.\ hadr.}}$ are the responses of the electromagnetic and the hadron calorimeters to neutral and charged hadrons, and $\mathrm{E}C_{e/\gamma}$ is the response of the electromagnetic calorimeter to electrons and photons, respectively.

Assuming that all tracks are reconstructed, the reconstructed jet energy after subtraction becomes

$$E^{\mathrm{cor}}_{\mathrm{jet}} = \mathrm{EC}_{e/\gamma} + (\mathrm{EC} + \mathrm{HC})_{\mathrm{neutr.\ hadr.}} + E^{\mathrm{in\text{-}cone}}_{\mathrm{tracks}}. \tag{4}$$

After the addition of out-of-cone tracks, the final expression is

$$E^{\mathrm{cor}}_{\mathrm{jet}} = \mathrm{EC}_{e/\gamma} + (\mathrm{EC} + \mathrm{HC})_{\mathrm{neutr.\ hadr.}} + E^{\mathrm{in\text{-}cone}}_{\mathrm{tracks}} + E^{\mathrm{out\text{-}of\text{-}cone}}_{\mathrm{tracks}}. \tag{5}$$

The track reconstruction inefficiency leads to the appearance of an additional term in the expression for the corrected jet energy

$$E^{\mathrm{cor}}_{\mathrm{jet}} = \mathrm{EC}_{e/\gamma} + (\mathrm{EC} + \mathrm{HC})_{\mathrm{neutr.\ hadr.}} + E^{\mathrm{in\text{-}cone}}_{\mathrm{tracks}} + \\ + E^{\mathrm{out\text{-}of\text{-}cone}}_{\mathrm{tracks}} + (\mathrm{EC} + \mathrm{HC})^{\mathrm{no\ track}}_{\mathrm{charg.\ hadr.}}. \tag{6}$$

The variance of the distribution of $E^{\mathrm{cor}}_{\mathrm{jet}}$ can be expressed with the formula

$$D(E^{\mathrm{cor}}_{\mathrm{jet}}) = D(E^{\mathrm{rec}}_{\mathrm{jet}}) + \sum_{\mathrm{tracks\ out\ of\ cone}} D(E^{\mathrm{out\text{-}of\text{-}cone}}_{\mathrm{track}}) + \\ + \sum_{\mathrm{tracks\ in\ cone}} D(E^{\mathrm{exp}}_{\mathrm{track}}) + \sum_{\mathrm{tracks\ in\ cone}} D(E^{\mathrm{in\text{-}cone}}_{\mathrm{track}}), \tag{7}$$

$D(E^{\mathrm{in\text{-}cone}}_{\mathrm{tracks}})$ and $D(E^{\mathrm{out\text{-}of\text{-}cone}}_{\mathrm{tracks}})$ are defined by the tracker resolution which is negligible ($< 0.01 P^{\mathrm{track}}_{T}$) in comparison with $D(\langle E^{\mathrm{rec}}_{\mathrm{jet}}\rangle)$; $D(\langle E^{\mathrm{exp}}_{\mathrm{tracks}}\rangle)$ will go to zero as the size of the sample of prompt isolated particles is increased.

The jet energy resolution is defined with the formula

$$\text{Resolution}(E) = \sigma \frac{\left(E_{\text{jet}}^{\text{rec}}/E_{\text{jet}}^{\text{gen}}\right)}{\left\langle E_{\text{jet}}^{\text{rec}}/E_{\text{jet}}^{\text{gen}}\right\rangle} \tag{8}$$

where $E_{\text{jet}}^{\text{gen}}$ is the energy of generator jet.

The transverse jet energy resolution is defined with the formula

$$\text{Resolution}(E_T) = \sigma \frac{\left(E_{T\text{jet}}^{\text{rec}}/E_{T\text{jet}}^{\text{gen}}\right)}{\left\langle E_{T\text{jet}}^{\text{rec}}/E_{T\text{jet}}^{\text{gen}}\right\rangle} \tag{9}$$

Taking into account that the polar angle of jet direction θ is limited to the range from 15 to 90° and assuming that $\langle E \sin(\theta)\rangle \simeq \langle E\rangle\langle\sin(\theta)\rangle$, the transverse jet energy resolution can be expressed by the formula

$$\text{Resolution}(E_T) \simeq \sqrt{\text{Resolution}^2(E) + \cot^2(\theta) \times D(\theta)}, \tag{10}$$

where θ is the polar angle of jet direction and $\text{Resolution}(E)$ is defined with formula (8). The procedure increases the jet energy due to an exchange of the underestimated response of calorimeters to charged hadrons with the momentum of the track in the tracker and adding the out-of-cone energy. The variance is kept at the same value. The procedure results in decreasing of the first term of formula (10). The direction of jet is also corrected with the use of the primary vertex position and charged particles trajectory parameters. The correction of jet direction leads to decreasing of the second term of formula (10). The relative weights of the first and the second terms in formula (10) depend on the polar angle θ. The first term plays the main role in the barrel part of the CMS detector, while the second term dominates in the endcap.

The systematic shift $\delta E^{\text{syst}} = \langle E_{\text{jet}}^{\text{cor}}\rangle - \langle E_{\text{jet}}^{\text{gen}}\rangle$ has two possible origins, denoted δE_1, δE_2. The δE_1 contribution results from the uncertainty in the expected response parametrization. The δE_2 shift arises from neutral hadrons (and, equivalently, from charged hadrons with no associated track), the response of which is not corrected a posteriori.

Algorithm performance was tested in the sample of the single jets, the sample of the QCD jets in the different $\hat{p_T}$ bins in the low luminosity conditions and in the sample with dijet resonances in the low luminosity conditions.

3.4. Reconstruction of Single Jet [14]. Samples of QCD dijet events in different intervals of the initial parton transverse momentum, $\hat{p}_T$, were simulated with PYTHIA 6.158 [11]. At the generator level, jets are found with a simple cone algorithm ($R = 0.5$) around the leading particle in the jet. Particles belonging to the jet are passed through the complete detector simulation; other particles in the event are ignored. The calorimeter digitization is done in the no pile-up scenario (only one jet in detector).

The energy resolution (10) and the reconstructed energy dependence on the generated transverse energy are shown in Figs. 6 and 7 for jets generated with $|\eta| < 0.3$.

When the jet energy corrections are applied, the reconstructed jet energy fraction for 20 GeV generator jets increases from 0.5 to 0.85 and the same fraction for 120 GeV jets

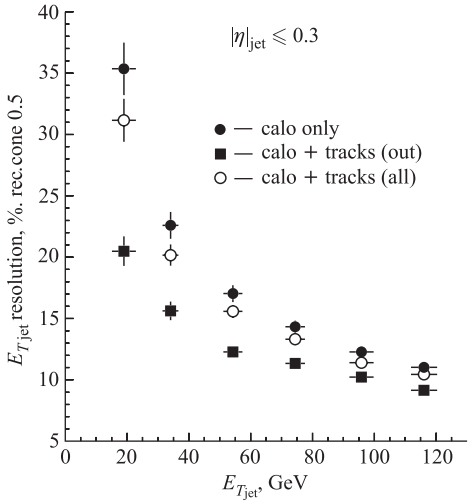

Fig. 6. The jet transverse energy resolution as a function of the original jet transverse energy in a single jet sample; reconstruction with calorimeter only (closed circles), subtraction procedure of expected responses using library of responses and out-of-cone tracks [14]

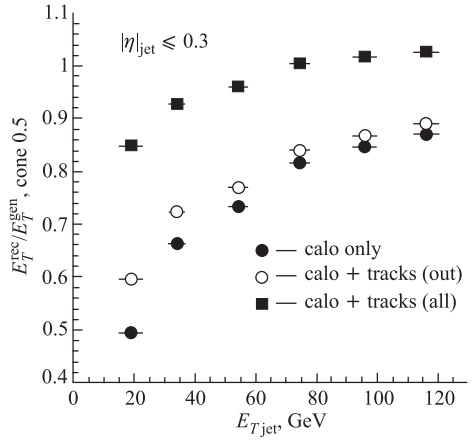

Fig. 7. Reconstructed jet transverse energy as a function of the generator jet transverse energy in a single jet sample; reconstruction with calorimeter only (closed circles), out-of-cone tracks (open circles), subtraction procedure of expected responses using library of responses [14]

increases from 0.87 to 1.03 (Fig. 7). The resolution improves in 1.7 times for jets with transverse energy of 20 GeV in barrel and up to 15% for jets with transverse energy of 100 GeV (Fig. 6). Complete linearity restoring is possible taking into account the systematical uncertainties connected with tracking inefficiency for charged hadrons, thresholds effects and Monte-Carlo corrections for the energy deposited by neutral hadrons.

3.5. Reconstruction of QCD Jet Events in the Low Luminosity Conditions [14]. Dijet events with $\hat{p}_T$ between 80 and 120 GeV/c were generated with PYTHIA 6.158 fully simulated, digitized and reconstructed in low-luminosity conditions ($\mathcal{L} = 2{\cdot}10^{33}\,\text{cm}^{-2}{\cdot}\text{s}^{-1}$) using detailed description of CMS. Average number of additional minimum bias events in one pile-up for

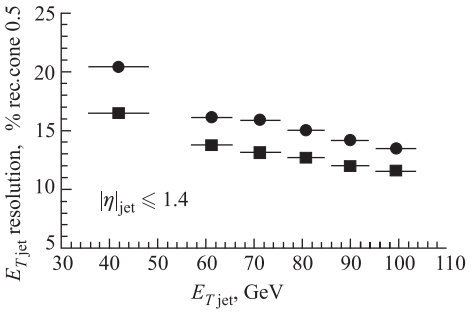

Fig. 8. Jet transverse energy resolution as a function of the generator jet transverse energy for jets with $0 < |\eta| < 1.4$ (barrel) from a sample with low luminosity pile-up; reconstruction with calorimeter only (closed circles), subtraction procedure of expected responses using library of responses and out-of-cone tracks (closed squares) [14]

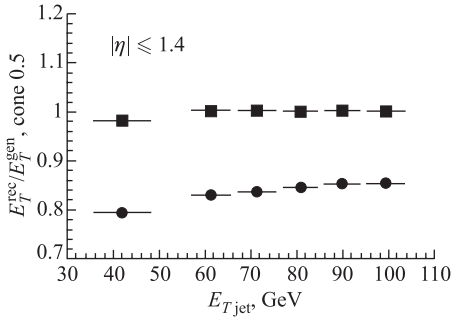

Fig. 9. Reconstructed jet transverse energy as a function of the generator jet transverse energy. The symbols are the same as in Fig. 8 [14]

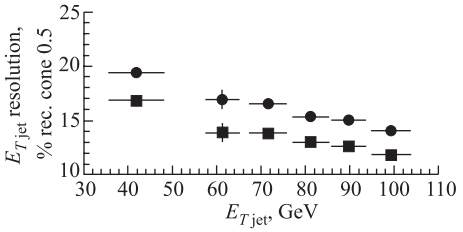

Fig. 10. Jet transverse energy resolution as a function of the generator jet transverse energy for jets with $1.4 < |\eta| < 3.0$ (endcap) from a sample with low luminosity pile-up; reconstruction with calorimeter only (closed circles), subtraction procedure of expected responses using library of responses and out-of-cone tracks (closed squares) [14]

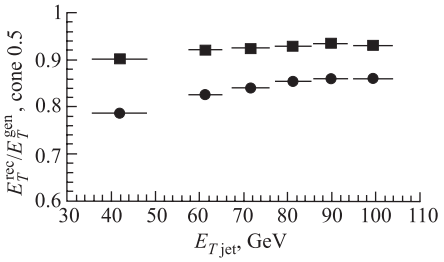

Fig. 11. Reconstructed jet transverse energy as a function of the generator jet transverse energy. The symbols are the same as in Fig. 10 [14]

one hard interaction is 3.5. The resolution and the reconstructed jet energy fraction are shown for jets generated with $|\eta| < 1.4$ in Figs. 8 and 9 and in the endcaps in Figs. 10 and 11. This sample was simulated with pile-up events and no special procedures to suppress pile-up energy were used. The resolution improvement is the same as for single jets with no pile-up. A larger amount of energy is however present in the jet cone R_{rec}. This amount is the same for all jet energies and corresponds to the energy flow average from the pile-up events. The additional energy affects lower-energy jets more than higher-energy jets. The dependence on the generator transverse jet energy is therefore less pronounced. Jets in the endcap are more affected by pile-up than in the barrel.

3.6. Reconstruction of the Dijet Resonances in the Low Luminosity Conditions [14]. Events with a 120 GeV/c^2 Z' decaying into light quarks with initial state and final state radiation were fully simulated, digitized and reconstructed for low luminosity pile-up conditions. The X mass is reconstructed from the two leading jets that are within $R = 0.5$ of the direction of the primary partons. The mass peak for the generated mass is at 115 GeV/c^2 and the mean value is 110 GeV/c^2. The same jets reconstructed in the calorimeters only give the mass peak at 96 GeV/c^2. A ratio of the Z' mass reconstructed to the Z' mass generated for calorimetry jets and calorimeter-plus-tracker jets is shown in Fig. 12.

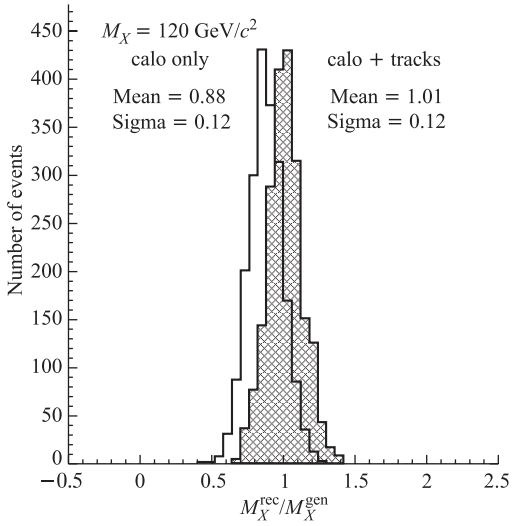

Fig. 12. Ratio of the reconstructed to the generated X mass with calorimeters only (empty histogram) and with calorimeter + tracks corrections (hatched histogram) [14]

The dijet mass is restored with a systematic shift of about 1% and the resolution is improved by 10%. The ratio of the reconstructed to the generated X mass is 0.88 before corrections with tracks and 1.01 after corrections. The calculation of the pile-up events contribution to the mass spectrum is done with a simple estimate. Taking into account that pile-up events add on average $\Delta E \approx 2.5$ GeV [15] in a cone with $R = 0.5$ to the jet energy, the contribution of the pile-up energy to the mean reconstructed mass is estimated to be ≈ 5 GeV/c^2 ($\langle M_{\text{pile-up}} \rangle \approx \langle M \rangle + 2\Delta E$). After subtraction of the additional pile-up energy (≈ 2.5 GeV) from the reconstructed jet energy, the ratio of the reconstructed to the generated masses is 0.84 and 0.97 before and after applying corrections, respectively.

CONCLUSION

Methods of the jet energy corrections presented in the review, together with the calibration of the calorimeter towers with test-beams and sources, will be used both during the initial calibration and monitoring of HCAL towers and for jet energy corrections.

The following procedures have been identified for verifying the calorimeter tower calibration:

- Measure noise with beam-crossing triggers to check and adjust thresholds.
- Take data without zero-suppression to study nonlinear effects connected with thresholds.
- Check and adjust symmetry with minimum bias trigger.
- Use isolated muons from W decays to compare tower-to-tower response to radioactive source measurements and test-beam muons.
- Compare isolated high-p_T tracks with test-beam data.

The following procedure will be used to check the calibration of jets:

• Measure the effect of pile-up on the jet reconstruction algorithms and thresholds using data without zero-suppression.

• Use p_T balance between γ and jet to calibrate the absolute energy scale.

• Use p_T balance in dijet events to calibrate the jet energy vs η and verify the resolution.

• Use $W \to jj$ mass fitting in tagged $t\bar{t}$ events to check and fine tune the jet energy scale.

• Use the jet energy correction using tracks to estimate the response of the calorimeter to the particle flow in the definite cone.

Using the combination of the different methods, the systematical shift of the absolute scale can be set 10% for jets with energy less than 40 GeV and 3–5% for jets with transverse energy above 80–100 GeV.

REFERENCES

1. CMS ECAL Technical Design Report. CERN/LHCC 97-33. 1997;
   CMS HCAL Technical Design Report. CERN/LHCC 97-31. 1997;
   CMS Technical Tracker Design Report. CERN/LHCC 98-6. 1998.
2. *Abramov V. V. et al.* Studies of the Response of the Prototype CMS Hadron Calorimeter, Including Magnetic Field Effects, to Pion, Electron and Muon Beams. CMS NOTE 2000/003. 2000.
3. *Wigmans R.* // Nucl. Instr. Meth. A. 1988. V. 265. P. 273.
4. *Akchurin N. et al.* // Nucl. Instr. Meth. A. 1997. V. 399. P. 202–226.
5. CMS TriDAS Project Data Acquisition and High-Level Trigger Technical Design Report. CERN/LHCC 2002-26 CMS TDR 6.2.
6. Physics Technical Design Report. V. 1. CERN/LHCC 2006-001.
7. *Blazey G. C. et al.* Run II Jet Physics // Proc. of the Workshop «QCD and Weak Boson Physics in Run II» / Ed. by Baur U., Ellis R. K., Zeppenfeld D. P. 47.
8. *Ellis S. D., Soper D. E.* Successive Combination Jet Algorithm for Hadron Collisions // Phys. Rev. D. 1993. V. 48. P. 3160; hep-ph/9305266.
9. *Accardi A. et al.* Yellow Report CERN 2004-009. Jet Chapter.
10. *Agostinelli S. et al. (GEANT4 Collab.).* GEANT4: A Simulation Tool Kit // Nucl. Instr. Meth. A. 2003. V. 506. P. 250–303. doi:10.1016/S0168-9002(03)01368-8.
11. *Sjostrand T.* // Comp. Phys. Commun. 2001. V. 135. P. 238.
12. *Heister A. et al.* CMS NOTE-2006/036. 2006.
13. *Konoplianikov V., Kodolova O., Ulyanov A.* CMS NOTE-2006/042.
    http://dx.doi.org/10.1140/epjcd/s2006-02-003-9
14. *Kodolova O. et al.* CMS NOTE-2004/015. 2004; http://dx.doi.org/10.1140/epjcd/s2005-02-004-2
15. *Nikitenko A., Kunori S., Kinnunen R.* Missing Transverse Energy Measurement with Jet Energy Corrections. CMS NOTE 2001/040. 2001.

Received on September 21, 2006.